

Temperature Field Validation on Supercritical Coaxial Injection

Leandro B. Magalhães^{†}, André R. R. Silva^{*} and Jorge M. M. Barata^{*}*

^{}AEROG-LAETA University of Beira Interior
Covilhã 6201-001, Portugal*

leandro.magalhaes@ubi.pt · andre@ubi.pt · jbarata@ubi.pt

[†]Corresponding author

Abstract

In the present manuscript, we report on the numerical simulation of coaxial nitrogen injection under subcritical and supercritical conditions, where the inner stream is recessed concerning the coaxial one. An incompressible but variable density description of supercritical phenomena is pursued as an alternative to more established compressible formulations, in which we extend past analysis focusing on the evaluation of density to the temperature field validation, according to the available experimental data. The results indicate that recirculation regions are formed as expected at either the inner jet axis or at the post tip between both streams. Furthermore, it is found that the transition threshold between the blockage effect depends on the momentum ratio and differs between subcritical and supercritical conditions.

1. Introduction

The increasing performance demands of liquid rocket engines (LREs) have led to conditions in the combustion chamber exceeding the critical point of both the fuels and oxidizers to pursue higher specific impulses. In contrast to solid propelled rocket engines, LREs offer higher specific impulses and launch abort capabilities. Generally, a rocket engine operates as an energy conversion system⁷ through the release of propellants' molecules' internal energy, its acceleration, and release through the bell-shaped nozzle.

A simple thermodynamic analysis of a rocket thrust chamber shows that the rocket size may decrease as pressure increases. However, this results in higher thrust chamber stresses and heat transfer rates. For combustion, increased chamber pressure decreases dissociation of the molecules and increases effective heat release, leading to higher specific impulse.⁴ Increasing pressure and temperature of propellants leads to conditions at injection and in the combustion chamber exceeding the critical points of fuels and oxidizers characteristic of mixing at supercritical conditions.

The critical point delimits the supercritical regime and is characterized by pressure and temperature values that become identifiers in the case of pure fluids. Thermodynamic singularities, which refer to the singular behavior of thermodynamic properties at the critical point, need to be accurately replicated in any numerical effort dedicated to successfully describing supercritical fluid behavior. When the isobaric-specific heat becomes infinite, the surface tension and latent heat become zero. Since the kinematic viscosity of supercritical fluids is lower than that of correspondent liquid and gas phases,¹⁰ the Reynolds number is conversely higher than that of corresponding liquid and gas phases for the same velocity, potentiating the formation of a turbulent flow. Besides, the discontinuity between the liquid and gas phases observed at subcritical conditions disappears, resulting in single-phase behavior under supercritical conditions.² In such situations, the injection cannot be thought of as leading to spray formation but as describing a fluid-fluid mixing process.¹⁹ Nevertheless, single-phase behavior does not imply a uniform behavior across the supercritical regime. Banuti and Hannemann¹ introduce the concept of thermal disintegration as complementary to the pure mechanical description of supercritical jet disintegration.

The need for quantitative experimental data sets cannot be understated since these allow for the validation of computational codes, reducing the trial-and-error phase in developing a propulsion system. Unfortunately, quantitative experimental data are hard to obtain given the difficulties encountered due to the harsh conditions of combustion chambers. The behavior of supercritical mixing and combustions can be significantly enhanced through cold flow or combustion experiments. Quantitative cold flow data provides insight into jet mixing at supercritical conditions without introducing the complexities of combustion and thermal equilibrium effects. These studies are usually conducted resorting to the Raman scattering technique,^{20,23,24} and while they detail the injection and mixing of nitrogen into a

SUPERCRITICAL INJECTION TEMPERATURE FIELD

quiescent nitrogen environment at supercritical or transcritical (temperature below the critical point) conditions, only information regarding the density field is available, leaving the temperature field validation as an open question.

The coaxial injection is a subject less understood than single injection configurations.²⁹ Mainly, for supercritical shear coaxial injection, the experiments of Davis and Chehroudi⁶ constitute the most extensive quantitative database of coaxial injection analysis, ranging from subcritical to supercritical conditions. For instance, Hosangadi et al.⁹ use a hybrid LES/RANS model to evaluate the coupling between turbulence mixing and non-linear thermodynamic properties and how it contributes to enhanced mixing at supercritical conditions, while Schmitt et al.²⁸ focus on the influence of injector geometry and the operating conditions. Their LES simulations show that when the momentum ratio is higher than a given threshold, the inner potential core breaks abruptly due to the formation of a recirculation zone close to the injector exit plane.

More recently, the coaxial injection configuration was looked into by Poormahmood and Farshchi.²⁶ Once again, LES is studied with the focus being on the finger-like structures formation and the effect turbulence has on the peak in isobaric-specific heat, labeled as a 'thermal shield'. Another relevant study to this discussion is the one of Liu et al.,¹⁴ where the focus is given to the modeling of acoustic excitation and its influence on near injector flow at higher injection velocities, coincident to those of the space shuttle main engine (SSME) pre-burner.

In the past¹⁵⁻¹⁸ our research group focused on the application of an incompressible but variable density approach³ to the modeling of supercritical and transcritical injection phenomena. These studies were, however, restricted to the density field evaluation, given the available experimental data. As such, in the present paper, we will focus on the temperature field evaluation under subcritical and supercritical conditions of nitrogen in a coaxial injection configuration at varying momentum and velocity ratios between the inner and outer streams.

2. The Experiment

The experimental conditions of Davis and Chehroudi⁶ describing the coaxial injection of nitrogen into a quiescent nitrogen environment are considered.

The computational domain is represented in Figure 1 depicting the position of the central and coaxial streams, indicating that the main stream is recessed concerning the coaxial one. The recess in oxygen-hydrogen coaxial injection contributes to flame stabilization inside the injector, enhancing the flame angle and increasing the reacting region, leading to a fast jet breakup. Establishing the parallel between this case with the non-reacting coaxial configuration studied in this jet, the heat transfer inside the injector is expected to assume a more preponderant role than in the single injection configurations.¹

In a typical rocket combustor, fuel and oxidizer are injected into the chamber through coaxial injectors whose performance is influenced by the absolute pressure being the velocity ratio of the outer-to-inner jet is a fundamental design parameter.

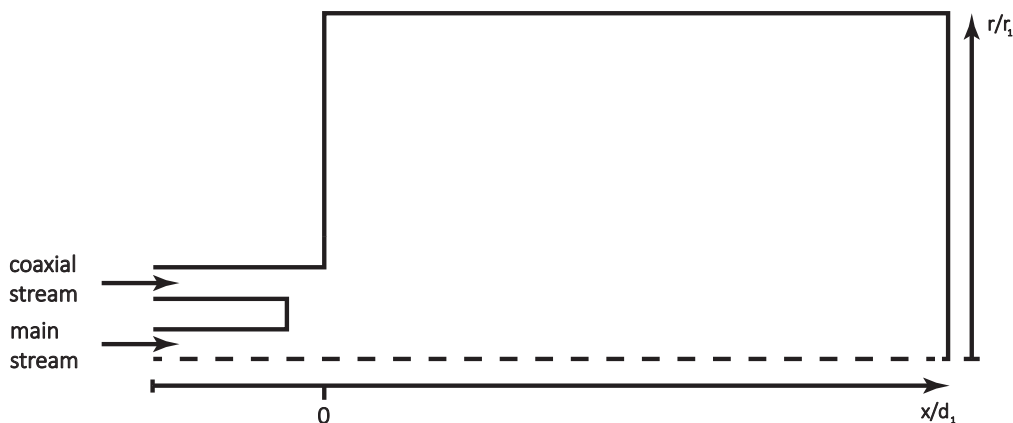


Figure 1: Coaxial geometry configuration.

The inner tube has a length of 50 mm, with an inner diameter, d_1 of 0.508 mm and an outer diameter, d_2 , of 1.59 mm, while the outer tube has an inner diameter, d_3 , of 2.42 mm and an outer diameter, d_4 of 3.18 mm. The inner tube is recessed concerning the outer tube by a length of half the inner tube inner diameter, d_1 . On the other hand, the combustion chamber has a length of 59.4 mm, with a height of 76 mm and a depth of 12.7 mm.

Radial temperature profiles are measured with a type-E thermocouple mounted on a traverse used to switch the thermocouple's position. The thermocouple bead has a diameter of 0.10 mm, and it is positioned at a distance

of 0.14 mm from the injector exit plane, while steady-state conditions are maintained in the experimental facility for each test case.⁶

Table 1 details the experimental test cases considered in the present study. Cases 1, 2, 3, and 4 correspond to injection under subcritical conditions, while cases 9, 10, 11, and 12 respect injection under supercritical conditions. p represents pressure, T the temperature, v the velocity, while VR and M denote outer-to-inner stream velocity and momentum ratios. Lastly, subscripts ∞ , i , and o correspond to conditions in the chamber, inner and outer streams, respectively.

Table 1: Conditions for the high outer-jet temperature cases.⁶

Case	p_∞ [MPa]	T_∞ [K]	T_i [K]	T_o [K]	v_i [m s ⁻¹]	v_o [m s ⁻¹]	VR [-]	M [-]
1	1.49	238	109	195	2.2	4.5	2.1	0.2
2	1.59	248	110	201	2.2	10.9	4.9	1.1
3	1.45	249	108	204	2.2	19.8	9.1	3.2
4	1.49	237	108	202	2.2	23.9	11.0	4.9
9	4.97	240	128	188	2.9	4.4	1.5	0.5
10	4.95	237	129	190	3.0	10.9	3.6	2.7
11	4.94	228	133	185	3.9	16.8	4.3	5.1
12	4.94	233	132	191	3.6	22.5	6.3	9.6
13	1.45	231	109	132	2.2	10.3	4.7	1.5

3. Formulation

The Favre averaged conservation equations for mass, momentum and energy are then represented in equations (1), (2) and (3), respectively.

$$\frac{\partial \bar{\rho} \tilde{u}_i}{\partial x_i} = 0 \quad (1)$$

$$\frac{\partial}{\partial x_j} \bar{\rho} \tilde{u}_i \tilde{u}_j = -\frac{\partial \bar{p}}{\partial x_i} + \frac{\partial \bar{\tau}_{ij}}{\partial x_j} - \frac{\partial \bar{\rho} \tilde{u}_i'' \tilde{u}_j''}{\partial x_j} \quad (2)$$

$$\frac{\partial \bar{\rho} \tilde{u}_j \tilde{H}}{\partial x_j} = \frac{\partial \bar{\tau}_{ij} \tilde{u}_i}{\partial x_j} - \frac{\partial \tilde{u}_i \bar{\rho} \tilde{u}_i'' \tilde{u}_j''}{\partial x_j} - \frac{\partial (\bar{q}_j + \bar{\rho} \tilde{u}_j'' \tilde{h}'')}{\partial x_j} \quad (3)$$

x_i and x_j represent the Cartesian coordinates, ρ the density, u_i and u_j the velocity components in the i th direction, p the pressure, τ_{ij} the viscous stress tensor, q_j the heat flux and H the total enthalpy. The Reynolds stress tensor and the turbulence heat flux are given in equations (4) and (5), where Pr_t is the turbulence Prandtl number and c_p the isobaric specific heat. The system is closed with the standard κ - ϵ turbulence model¹¹ with additional transport equations for the turbulence kinetic energy (κ) and its dissipation (ϵ).

$$\bar{\tau}_{ij} = \tilde{\mu} \left(\frac{\partial \tilde{u}_i}{\partial x_j} + \frac{\partial \tilde{u}_j}{\partial x_i} - \frac{2}{3} \delta_{ij} \frac{\partial \tilde{u}_k}{\partial x_k} \right) \quad (4)$$

$$\bar{\rho} \tilde{u}_j'' \tilde{h}'' = -\frac{c_p \mu_t}{Pr_t} \frac{\partial \tilde{T}}{\partial x_j} = -\frac{\mu_t}{Pr_t} \frac{\partial \tilde{h}}{\partial x_j} \quad (5)$$

Thermophysical properties like the dynamic viscosity, μ , the thermal conductivity, λ , density, and pressure are related to mass, momentum, and energy transport through an appropriate equation of state and suitable models taking into account departure functions accounting for real gas effects.

The Peng-Robinson²⁵ equation of state is used in the present work. It is given in equation 6, where v is the molar volume, R the gas constant, $a(T)$ the molecular attractive potential dependent upon temperature and b the repulsive potential. Auxiliary parameters such as attractive and repulsive potentials and relationship with the acentric factor, ω , are defined in equations (7) to (10).

$$p = \frac{RT}{v-b} - \frac{a(T)}{v(v+b) + b(v-b)} \quad (6)$$

SUPERCRITICAL INJECTION TEMPERATURE FIELD

$$a(T) = a(T_c).a(T_r, \omega) \quad (7)$$

$$a(T_c) = 0.45724 \frac{R^2 T_c^2}{p_c} \quad (8)$$

$$a(T_r, \omega) = \left[1 + (0.37464 + 1.54226\omega - 0.26992\omega^2) (1 - \sqrt{T_r}) \right]^2 \quad (9)$$

$$b = b_c = 0.07780 \frac{RT_c}{p_c} \quad (10)$$

Considering the Peng-Robinson²⁵ equation of state used, the definition of a thermal equation of state in terms of any given thermodynamic potential, such as, for instance, internal energy or enthalpy, is a straightforward process. Departure functions are exact descriptions of the thermodynamic variable because they are state variables, depending only on initial and final states and not on the path between them,⁸ being the only constraint in terms of hypothesis or approximations, the choice of the equation of state.

Enthalpy in equation (11) is derived according to Maxwell's relations and the fundamental laws of thermodynamics.²⁷ It is evaluated by adding to the ideal gas contribution (subscript zero) a departure function that accounts for real gas effects (the second term on the right-hand side of equation (11)). Ideal gas enthalpy is evaluated from the seven coefficient NASA polynomials.²¹

$$h(p, T) = h_0(T) + \int_{p_0}^p \left[\frac{1}{\rho} + \frac{T}{\rho^2} \left(\frac{\partial \rho}{\partial T} \right)_p \right] dp \quad (11)$$

Taking into account the Peng-Robinson,²⁵ enthalpy is explicitly evaluated from equation (12).

$$\frac{h(p, T) - h_0(T)}{\mathcal{R}} = \frac{a(T)a(T_r, \omega) + T \frac{\partial a}{\partial T}}{\mathcal{R}T \sqrt{8b^2}} \ln \left(\frac{2v + 2b - \sqrt{8b^2}}{2v + 2b + \sqrt{8b^2}} \right) - 1 + Z \quad (12)$$

Where:

$$\frac{\partial a}{\partial T} = - \frac{(0.37464 + 1.54226\omega - 0.26992\omega^2) a(T_c)}{T_c T_r^{1/2}} \quad (13)$$

Similarly, the isobaric specific heat, c_p is defined in equation (14).

$$c_p(T, p) = c_v(T) - \frac{T \left(\frac{\partial p}{\partial T} \right)_v^2}{\left(\frac{\partial p}{\partial v} \right)_T} \quad (14)$$

Transport properties such as the thermal conductivity and dynamic viscosity are also evaluated through the departure function formalism following the models of Lemmon and Jacobsen.¹² For the dynamic viscosity, two terms are considered in equation (15), one for the ideal gas component ($\mu^0(T)$) and another for the real gas effects ($\mu^r(p, T)$). On the other hand, given thermal conductivity's (λ) critical divergence (equation (16)), a third term is included²² to improve its description.

$$\mu = \mu^0(T) + \mu^r(p, T) \quad (15)$$

$$\lambda = \lambda^0(T) + \lambda^r(p, T) + \lambda^c(p, T) \quad (16)$$

Following previous work^{3,18} a staggered grid configuration prevents pressure and velocity fields from decoupling, where pressure is directly evaluated from cell faces with no need for interpolation while preventing the appearance of oscillations. In addition, diffusive terms follow the second-order accurate central scheme, while advective terms follow the third-order accurate QUICK scheme,¹³ preventing the appearance of spurious pressure-induced oscillations caused by the equation of state formulation.

4. Validation

Figure 2 depicts the grid independence study for selected conditions. Radial temperature profiles are evaluated for each condition as a function of the radial distance from the jet centerline (r) normalized by the inner tube radius (r_1). The corresponding analysis of the computational error as the grid is progressively refined is given in Figure 3. The figure depicts two sets of experimental measurements denoted as positive and negative. They correspond to temperature values measured for positive⁶ r/r_1 and for negative⁵ r/r_1 measured from the jet centerline. Moreover, the chamber temperature is also depicted in the blue dashed line.

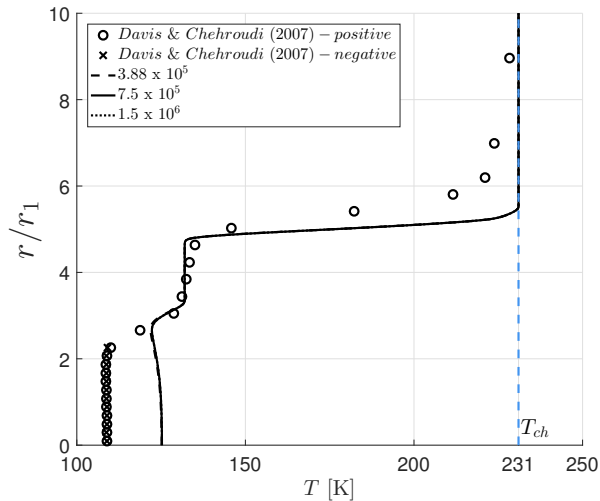


Figure 2: Grid Independence Study, corresponding to case 13 in subcritical conditions.

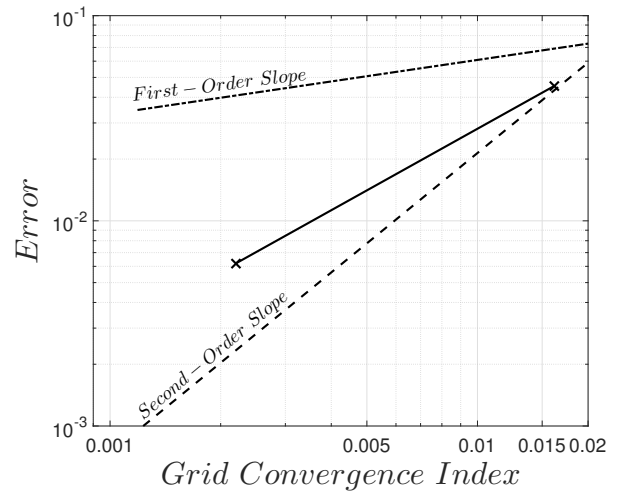


Figure 3: Error propagation, corresponding to case 13 in subcritical conditions.

5. Results

Figures 4, 5, 6 and 7 depict the comparisons between the experiments and the numerical results for cases 1, 2, 3 and 4, respectively. Through the analysis of the figures, it is possible to infer the momentum ratio threshold leading to the inner core breakup and the blockage effect of the recirculation. To the lower momentum ratio (0.2 in case 1), no recirculation blockage is discernible in Figure 4, where the experimental region of constant temperature is retrieved in the computations, albeit with different lengths. From here, the momentum ratio increases to 1.1 in case 2, and the blockage influence starts to be felt in the radial profiles, which exhibit similar behaviors to those of cases 14 and 15, as the momentum ratio is further increased in cases 3 and 4.

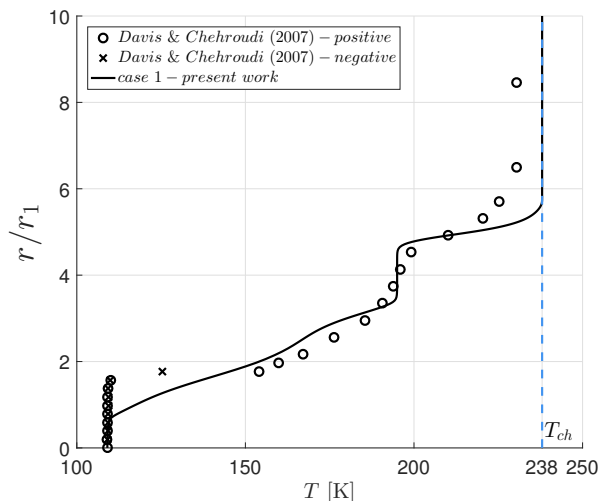


Figure 4: Radial temperature profile for case 1.

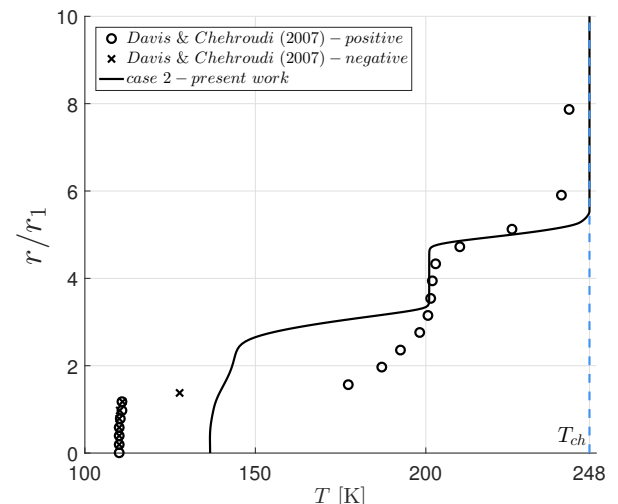


Figure 5: Radial temperature profile for case 2.

SUPERCRITICAL INJECTION TEMPERATURE FIELD

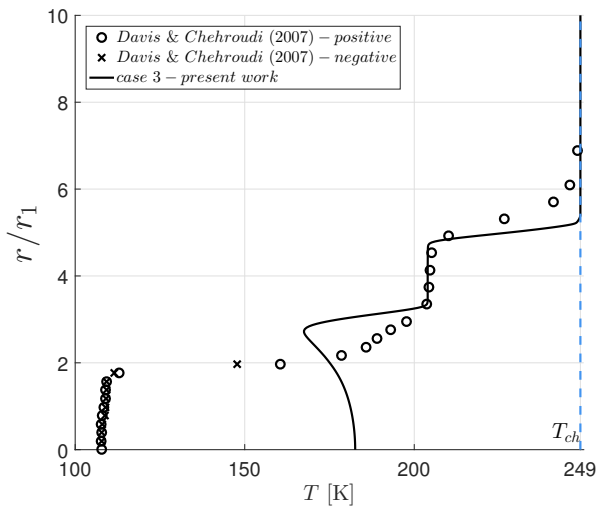


Figure 6: Radial temperature profile for case 3.

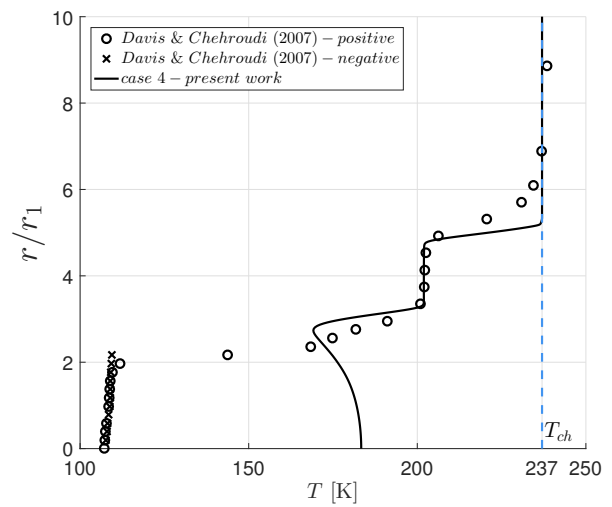


Figure 7: Radial temperature profile for case 4.

Figures 8 and Figure 9 depict the velocity fields of cases 1 and 4, respectively. Interestingly, in Figure 8 for a VR of 2.1 and a M of 0.2, it is possible to observe a distinct behavior than the one presented for the remaining subcritical conditions. Due to the low-momentum ratio of 0.2, there is no blockage effect due to the recirculation. Instead, two counter-rotating recirculations are anchored to the post tip between the two jets. The recirculation close to the inner jet rotates counter-clockwise, while a clockwise recirculation is observed closer to the outer jet.

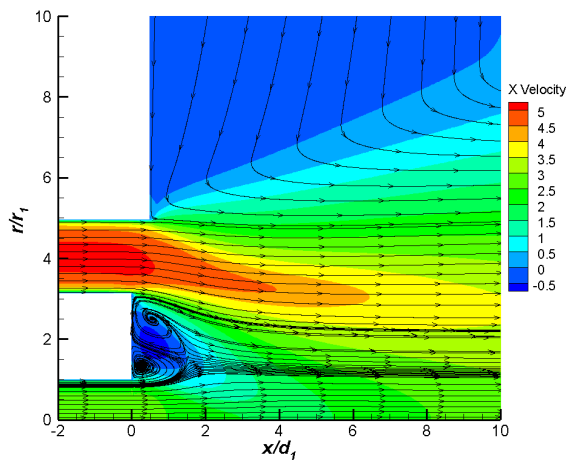


Figure 8: Case 1 velocity field and recirculation.

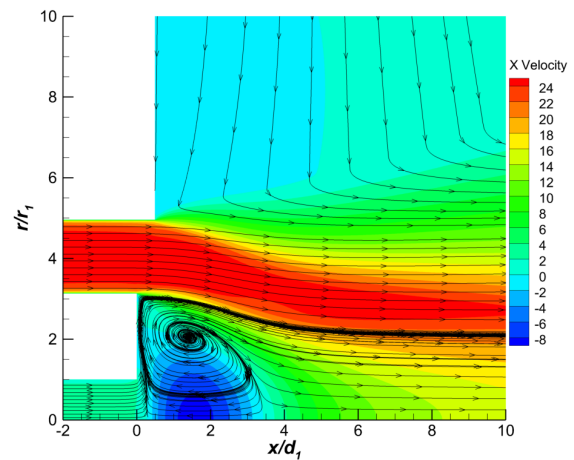


Figure 9: Case 4 velocity field and recirculation.

As the velocity and momentum ratios are further increased to 11.0 and 4.9, respectively, in Figure 9 a distinct behavior than case 1 is observed. However, as previously reported for the low outer-jet temperature cases in the preceding section, a similar flow structure is observed, that is, the inner jet blockage by the recirculation region.

At subcritical conditions, the increasing outer-to-inner velocity and momentum ratios promote the inner jet blockage, regardless of the low or high outer-jet injection temperature. On the other hand, differences between numerical computations and the experimental data are explained due to the intrusive measurement caused by the thermocouple and the traverse in which it is supported, especially given the dimensions of the recirculations and the thermocouple bead.

Radial temperature profiles are compared in Figures 10, 11, 12 and 13, corresponding to cases 9, 10, 11 and 12, respectively. Through the analysis of the figures, it was observed that as the momentum ratio, the size of the recirculation region formed at the post tip increases, similarly to the results obtained for the near-critical high outer-jet temperature cases, which again shows that the state in which the outer jet enters the chamber will greatly impact mixing and the coaxial jet evolution.

SUPERCRITICAL INJECTION TEMPERATURE FIELD

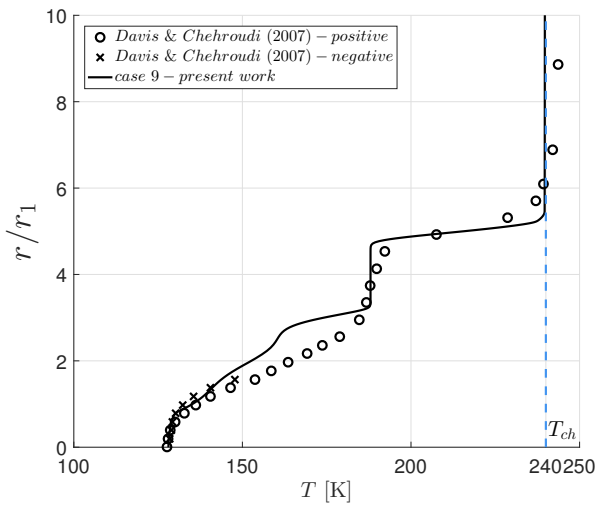


Figure 10: Radial temperature profile for case 9.

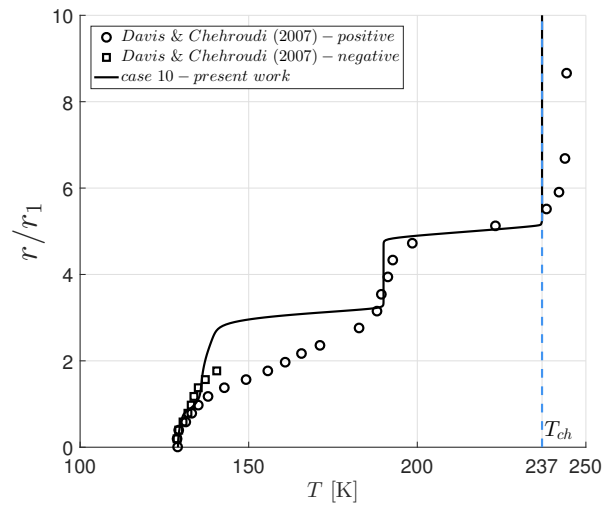


Figure 11: Radial temperature profile for case 10.

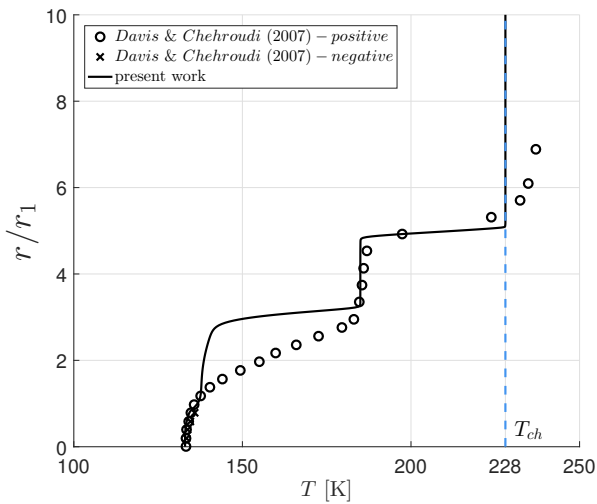


Figure 12: Radial temperature profile for case 11.

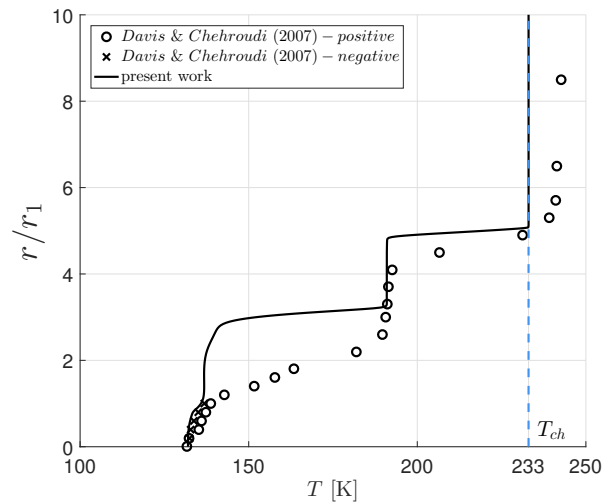


Figure 13: Radial temperature profile for case 12.

Figure 14 depicts the velocity field of case 10 with a VR of 3.6 and a M of 2.7 for supercritical inner jet injection conditions. Similar to case 1, two counter-rotating recirculations are observed at the post tip between the two jets. Increasing the velocity ratio to 4.3 and the momentum ratio to 5.1, similar velocity development to case 10 is depicted in Figure 15. Through the comparison of both fields, it is observed that the velocity ratio increase promoted the change in the position of the recirculations from x/d_1 of 2.5 to 3.0. It is impossible to observe the inner jet blockage at supercritical conditions, even for velocity ratios higher than two. This could be due to the temperature profile inside the injector and the different coupling mechanisms between subcritical and supercritical conditions added to the influence of surface tension at subcritical conditions.

SUPERCRITICAL INJECTION TEMPERATURE FIELD

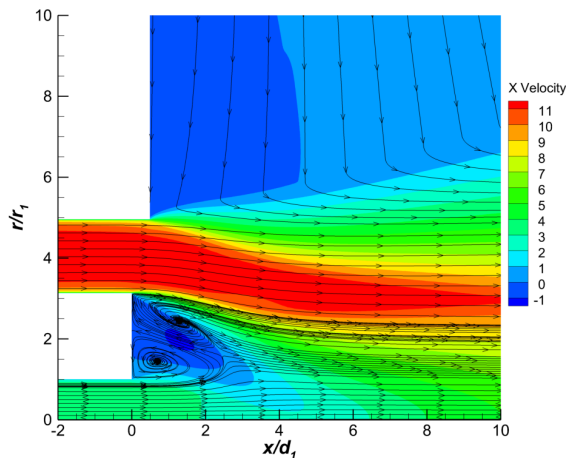


Figure 14: Case 10 velocity field and recirculation.

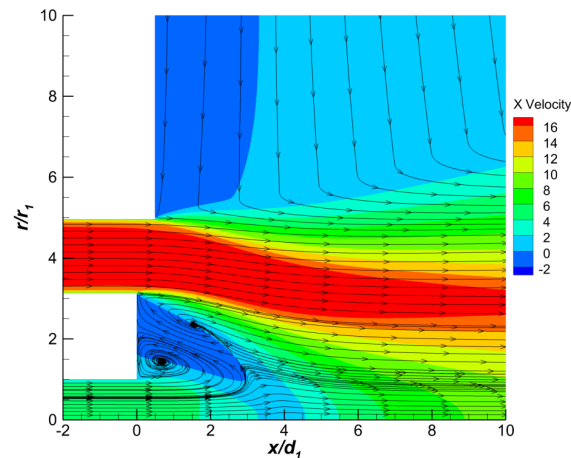


Figure 15: Case 11 velocity field and recirculation.

6. Conclusions

The evaluation of single species nitrogen injected through a shear coaxial injector where the main stream is recessed concerning the coaxial one was evaluated for conditions ranging from subcritical to supercritical for different temperatures and outer-to-inner velocity ratios. As a result, recirculation regions are formed at either the jet axis or the post between both jets, depending on the outer-to-inner jet momentum and velocity ratios. The transition threshold differs between injection under subcritical or supercritical conditions in terms of the outer-to-inner jet momentum ratio.

The velocity ratio effect is characterized by the temperature field evaluation at a broad range of conditions. As the outer stream velocity increases, mixing is enhanced, reducing the potential core length and increasing jet spreading, which is more pronounced in terms of temperature, demonstrating that heat propagation is dominant over momentum transport.

7. Acknowledgments

The present work was performed under the scope of activities at the Aeronautics and Astronautics Research Center (AEROG) of the Laboratório Associado em Energia, Transportes e Aeronáutica (LAETA), and was supported by the Fundação para a Ciência e Tecnologia, Portugal (Grant No. SFRH/BD/136381/2018, Project No. UIDB/50022/2020).

References

- [1] D. T. Banuti and K. Hannemann. The Absence of a Dense Potential Core in Supercritical Injection: A Thermal Break-up Mechanism. *Phys. Fluids*, 28(3):035103, 2016.
- [2] D. T. Banuti, M. Raju, C. Ma, M. Ihme, and J. Hickey. Seven Questions about Supercritical Fluids – Towards a New Fluid State Diagram. In *55th AIAA Aerospace Sciences Meeting*, AIAA paper 2017-1106, 2017.
- [3] J. Barata, I. Gökalp, and A. Silva. Numerical Study of Cryogenic Jets under Supercritical Conditions. *J. Propul. Power*, 19(1):142–147, 2003.
- [4] B. Chehroudi, D. Talley, and E. Coy. Initial Growth Rate and Visual Characteristics of a Round Jet into a Sub- to Supercritical Environment of Relevance to Rocket, Gas Turbine, and Diesel Engines. In *37th Aerospace Sciences Meeting and Exhibit*, AIAA paper 1999-0206, 1999.
- [5] D. Davis. *On the Behavior of a Shear-coaxial Jet, Spanning Sub- to Supercritical Pressures, with and without an Externally Imposed Transverse Acoustic Field*. PhD thesis, The Pennsylvania State University, 2006.
- [6] D. W. Davis and B. Chehroudi. Measurements in an Acoustically Driven Coaxial Jet under Sub-, Near-, and Supercritical Conditions. *J. Propul. Power*, 23(2):364–374, 2007.

- [7] O. J. Haidn. *Advances on Propulsion Technology for High-speed Aircraft*, chapter Advanced Rocket Engines, pages 6–40. NATO Research and Technology Organisation, 2008.
- [8] J. P. Hickey and M. Ihme. *Supercritical Mixing and Combustion in Rocket Propulsion*. resreport 12, Center for Turbulence Research, 2013.
- [9] A. Hosangadi, C. P. Lee, C. Kannepalli, and S. Arunajatesan. Three-dimensional Hybrid RANS/LES Simulations of a Supercritical Liquid Nitrogen Jet. In *44th AIAA/ASME/SAE/ASEE Joint Propulsion Conference & Exhibit*, AIAA paper 2008–5227, 2008.
- [10] Y. Ito. *Heat exchangers - advanced features and applications*, chapter Heat Transfer of Supercritical Fluid Flows and Compressible Flows, pages 125–147. InTech, 2017.
- [11] B. E. Launder and D. B. Spalding. *Lectures in Mathematical Models of Turbulence*. London, England: Academic Press, 1972.
- [12] E. W. Lemmon and R. T. Jacobsen. Viscosity and Thermal Conductivity Equations for Nitrogen, Oxygen, Argon and Air. *Int. J. Thermophys.*, 25(1):21–69, 2004.
- [13] B. P. Leonard. A Stable and Accurate Convective Modelling Procedure Based on Quadratic Upstream Interpolation. *Comput. Methods Appl. Mech. Eng.*, pages 58–98, 1979.
- [14] T. Liu, X. Wang, and V. Yang. Flow Dynamics of Shear-coaxial Cryogenic Nitrogen Jets under Supercritical Conditions with and Without Acoustic Excitations. *Phys. Fluids*, 33(7):076111, 2021.
- [15] L. Magalhães, F. Carvalho, A. Silva, and J. Barata. Turbulence Modeling Insights into Supercritical Nitrogen Mixing Layers. *Energies*, 13(7), 2020.
- [16] L. Magalhães, A. Silva, and J. Barata. Computational Study on Coaxial Nitrogen–Hydrogen Injection at Supercritical Conditions. In *AIAA Science and Technology Forum 2022*, AIAA paper 2022–0877 2022.
- [17] L. B. Magalhães, A. R. Silva, and J. M. Barata. Computational Analysis of High-Pressure Nitrogen Jets from Transcritical to Supercritical Gas-Like Conditions. In *AIAA Propulsion and Energy Forum*, AIAA paper 2021–3341 2021.
- [18] L. B. Magalhães, A. R. R. Silva, and J. M. M. Barata. Contribution to the Physical Description of Supercritical Cold Flow Injection: The Case of Nitrogen. *Acta Astronaut.*, (190):251–260, 2022.
- [19] W. Mayer, A. Schik, C. Schweitzer, and M. Schaeffler. Injection and mixing processes in high pressure LOX/GH2 rocket combustors. In *32nd Joint Propulsion Conference and Exhibit*, volume AIAA 96-2620, 1996.
- [20] W. Mayer, J. Telaar, R. Branam, G. Schneider, and J. Hussong. Raman Measurements of Cryogenic Injection at Supercritical Pressure. *Heat Mass Transfer*, 39(8-9):709–719, 2003.
- [21] B. J. McBride, M. J. Zehe, and S. Gordon. NASA Glenn Coefficients for Calculating Thermodynamic Properties of Individual Species. Technical Report NASA/TP–2002-211556, NASA Glenn Research Center, 2002.
- [22] G. A. Olchowy and J. V. Sengers. A Simplified Representation for the Thermal Conductivity of Fluids in the Critical Region. *Int. J. Thermophys.*, 10(2):417–426, 1989.
- [23] M. Oswald and A. Schik. Supercritical Nitrogen Free Jet Investigated by Spontaneous Raman Scattering. *Exp. Fluids*, 27(6):497–506, 1999.
- [24] M. Oswald, A. Schik, M. Klar, and W. Mayer. Investigation Of Coaxial LN2/GH2-injection at Supercritical Pressure by Spontaneous Raman Scattering. In *35th Joint Propulsion Conference and Exhibit*, AIAA paper 99–2887, 1999.
- [25] D. Peng and D. B. Robinson. A New Two-constant Equation of State. *Ind. Eng. Chem. Fundam.*, 15(1):59–64, 1976.
- [26] A. Poormahmood and M. Farshchi. Numerical Study of the Mixing Dynamics of Trans- and Supercritical Coaxial Jets. *Phys. Fluids*, 32(12):125105, 2020.
- [27] R. C. Reid, J. M. Prausnitz, and B. E. Poling. *The Properties of Gases and Liquids*. McGraw-Hill, Inc, 1987.

SUPERCRITICAL INJECTION TEMPERATURE FIELD

- [28] T. Schmitt, J. Rodriguez, I. A. Leyva, and S. Candel. Experiments and Numerical Simulation of Mixing under Supercritical Conditions. *Phys. Fluids*, 24(5):55–104, 2012.
- [29] R. van Hout, S. Murugan, A. Mitra, and B. Cukurel. Coaxial Circular Jets—A Review. *Fluids*, 147(6), 2021.